Eur. Phys. J. C (2023) 83:451
https://doi.org/10.1140/epjc/s10052-023-11548-1

THE EUROPEAN PHYSICAL JOURNAL C

Regular Article - Theoretical Physics

Dynamical galactic effects induced by solitonic vortex structure in bosonic dark matter

K. Korshynska[1,2,a], **Y. M. Bidasyuk**[2,b], **E. V. Gorbar**[1,3,c], **Junji Jia**[4,d], **A. I. Yakimenko**[1,5,6,e]

[1] Department of Physics, Taras Shevchenko National University of Kyiv, 64/13, Volodymyrska Street, Kyiv 01601, Ukraine
[2] Physikalisch-Technische Bundesanstalt (PTB), Bundesallee 100, 38116 Braunschweig, Germany
[3] Bogolyubov Institute for Theoretical Physics, 14-b Metrolohichna Street, Kyiv 03143, Ukraine
[4] School of Physics and Technology, Wuhan University, 299 Bayi Road, Wuhan, Hubei, China
[5] Dipartimento di Fisica e Astronomia 'Galileo Galilei', Universit'a di Padova, via Marzolo 8, 35131 Padua, Italy
[6] Istituto Nazionale di Fisica Nucleare, Sezione di Padova, via Marzolo 8, 35131 Padua, Italy

Received: 7 February 2023 / Accepted: 23 April 2023 / Published online: 31 May 2023

Abstract The nature of dark matter (DM) remains one of the unsolved mysteries of modern physics. An intriguing possibility is to assume that DM consists of ultralight bosonic particles in the Bose–Einstein condensate (BEC) state. We study stationary DM structures by using the system of the Gross–Pitaevskii and Poisson equations, including the effective temperature effect with parameters chosen to describe the Milky Way galaxy. We have investigated DM structure with BEC core and isothermal envelope. We compare the spherically symmetric and vortex core states, which allows us to analyze the impact of the core vorticity on the halo density, velocity distribution, and, therefore, its gravitational field. Gravitational field calculation is done in the gravitoelectromagnetism approach to include the impact of the core rotation, which induces a gravimagnetic field. As a result, the halo with a vortex core is characterized by smaller orbital velocity in the galactic disk region in comparison with the non-rotating halo. It is found that the core vorticity produces gravimagnetic perturbation of celestial body dynamics, which can modify the circular trajectories.

1 Introduction

The nature of DM particles remains one of the most fascinating puzzles of modern physics. The DM large-scale properties consistent with astrophysical observations are successfully explained by the cold dark matter model (CDM), which describes DM as a collisionless sufficiently cold perfect fluid. However, at smaller scales, the CDM encounters the cusp-core, missing satellites, and too-big-to-fail problems. One possibility to solve them is to assume that DM particles are ultra-light bosons as it is assumed in ultra-light dark matter (ULDM) models [1]. Generically, these models are characterized by the suppression of the small-scale structures, the presence of cores, and dynamic effects which arise from the BEC formed in the central regions of galaxies. Such DM halo proposals were investigated in [2–7].

The ULDM model is supported indirectly by observations. For example, in cosmological simulations [8] it was found that the bosonic DM can indeed reproduce the observed distribution of matter at very large scales [9,10], though the mass of such bosons should be extremely small. There have been also studies on some tensions of the ULDM with observational data from the rotation curves of galaxies including the Milky Way, which could probe the particle mass in the range $m = 10^{-22} - 10^{-21}$ eV [11,12]. Furthermore, the viability of the ULDM model was studied with the stellar kinematics measurements in dwarf galaxies [13]. Another important piece of evidence is the DM non-gravitational self-interaction, which has been recently reported for collisions of the clusters [14,15]. In addition, the DM halo model must ensure the stability of a predicted halo. The stability of compact astrophysical objects which may be formed due to the Bose–Einstein condensation of ULDM was shown numerically [16].

In the present paper, we discuss DM, which consists of ultra-light bosons with repulsive self-interaction. Such models make use of two macroscopic quantum phenom-

[a] e-mail: korshk0000a@gmail.com
[b] e-mail: yurabid@gmail.com
[c] e-mail: gorbar@bitp.kiev.ua
[d] e-mail: junjijia@whu.edu.cn (corresponding author)
[e] e-mail: alexander.yakimenko@gmail.com

ena: Bose–Einstein condensation and superfluidity. Bose–Einstein condensate in the mean-field approximation is described by the Gross–Pitaevskii equation. The finite temperature effects as well as thermal excitations are addressed in [17,18]. In particular, we point out that the finite temperature effects could lead to modification of the galactic halo density distribution. In our model, the contribution of thermal excitations can be safely neglected and the whole bosonic system can be described as BEC by using the Gross–Pitaevskii equation. By adding dissipation in the Gross–Pitaevskii equation one obtains a more general model, which includes the effective temperature effect and predicts that the ULDM halo consists of a BEC core and an isothermal envelope [19,20]. Such core-envelope structure in the ULDM model was also discussed in [21–24]. Another important property, superfluidity, allows the quantization of the circulation and thus the possibility of the formation of vortices in the core of the halo. The central object of our study, the vortex, has a vanishing wavefunction at the vortex line, with a quantized circular flow around the vortex line [1]. So the BEC can form self-sustained vortex solitonic structures with nonzero angular momentum and phase dislocation at the vortex core like those discussed in [25–28]. On the other hand, vortices can be induced by external rotation [29–31]. In the present work, we investigate nonlinear vortex soliton structures of self-gravitating BEC without any external rotation. According to the recent numerical studies [27,28] only the non-rotating soliton and single-charged vortex are stable, even when strongly perturbed. In the present work, we consider a DM halo, which consists of two regions - core and isothermal envelope, while the core could be either a soliton or a single-charged vortex.

Most of our knowledge about DM is based on its gravitational interaction with baryonic matter objects. Thus, testing the validity of the UDM theory requires a detailed investigation of the DM gravitational field. The DM density distribution, predicted by ULDM models, has been extensively studied in numerical simulations and applied in studies aimed at reconstructing the gravitational potential of DM halos for the Milky Way [32] and dwarf galaxies [33]. In general, one can determine the gravitational field of the ULDM by solving the Einstein equations with the DM density and rotation flow as sources of the gravitational field, where rotation flow is induced by the BEC superfluidity. Thus, in the ULDM model, we should be able to deduce the impact of the superfluid DM rotation on observations. The dominant effect of the vortex is due to its different core density distributions. Moreover, rotation flows produce v/c and higher order effects, which can be taken into account in the gravitoelectromagnetism approach discussed in [34–38] and used in our calculations below. The gravitoelectromagnetic formulation of a slowly rotating, self-gravitating, and dilute BEC intended for astrophysical applications in the context of DM halos was discussed in [39]. As a rule, the gravimagnetic force is quite weak and does not affect significantly the dynamics of astrophysical systems. However, in the central region of the BEC vortex core, the DM density vanishes while the vortex flow velocity dramatically increases, which can affect the dynamics of luminous matter in the central region of the galaxies.

In the present work, we calculate the DM gravitational field, which is needed for analysis of the observable predictions of the DM model, namely, to study how DM affects the movement of luminous matter. In our study, DM is the only source of a gravitational field, while luminous matter moves along geodesics, induced by DM. A more precise description of galactic kinematics is given by modeling the baryonic contribution to the gravitational potential which can distort the BEC soliton structures [40,41]. Such a contribution was found to be significant for the Milky Way (MW) but not essential for the SPARC LSB galaxies [42]. In this paper, we will limit ourselves to some simple consequences of the ULDM model on the galactic kinematics, namely, rotation curves and deviation of circular trajectory, induced by the gravimagnetic force. The more detailed study in this direction is beyond the scope of the current paper, though it is an interesting perspective on further work.

The paper is organized as follows. In Sect. 2, we develop the key parameters of our model, define the equations for halo structure, and formulate the gravitoelectromagnetism ansatz. In Sect. 3, we discuss the halo density profile for two stable core configurations and define the corresponding hydrodynamical velocity. In Sect. 4, the gravielectric (Newtonian) field of the halo is calculated and the rotational curves are obtained. Section 5 provides gravimagnetic field calculations and our estimates of the gravimagnetic effect on circular trajectory. The results are summarized in Sect. 6.

2 Model

2.1 Ultra-light dark matter model and halo structure

In this section, we briefly discuss the model suggested in [19,20]. The structure of the DM halo is described by the Gross–Pitaevskii–Poisson (GPP) equations, which define the dynamical evolution of self-gravitating BEC field ψ

$$
\begin{aligned}
i\hbar\frac{\partial\psi}{\partial t} = &-\frac{\hbar^2}{2m}\Delta\psi + m\Phi_{\rm g}\psi + \frac{K\gamma m}{\gamma-1}|\psi|^{2(\gamma-1)}\psi \\
&+\frac{m}{2}\left(\frac{3}{4\pi\eta_0}\right)^{2/3}|\psi|^{4/3}\psi + 2k_{\rm B}T_{\rm eff}\ln|\frac{\psi}{\psi_0}|\psi \\
&-i\frac{\hbar}{2}\xi\left[\ln\left(\frac{\psi}{\psi^*}\right) - \left\langle\ln\left(\frac{\psi}{\psi^*}\right)\right\rangle\right]\psi, \qquad (1)
\end{aligned}
$$

$$
\Delta\Phi_{\rm g} = 4\pi G|\psi|^2, \qquad (2)
$$

where $\langle X\rangle = \frac{1}{M}\int |\psi|^2 X d\mathbf{r}$ is the spatial average over the halo, m is the bosonic particle mass, $\hbar$ denotes the reduced Planck constant, k_B is the Boltzmann constant, $\psi_0 = \sqrt{\rho_0}$ with ρ_0 being a reference density and G is the gravitational constant.

The first equation can be obtained by incorporating dissipative effects into the Schrödinger equation by means of the theory of scale relativity [43]. This generalization of the Schrödinger equation means basically taking into account the interaction of the system with the environment. The more rigorous way to obtain the generalized GP equation is developed in [20], where the dissipation terms are explicitly derived by including the Lynden–Bell pressure. This pressure accounts for the gravitational cooling and violent relaxation phenomena and leads to configurations with a core-envelope structure. We follow this approach in our current work and point out its physical limitations: it describes a large-scale dilute many-particle bosonic system in the BEC state which is governed mainly by the self-gravitational interaction.

We consider the BEC model with parameters $\gamma = 2$ and $K = \frac{2\pi a_s \hbar^2}{m^3}$, where a_s denotes the s-wave scattering length of the self-interaction. The expression for K can be obtained by describing the scattering of bosons in the first Born approximation. This repulsive self-interaction is crucial for the stability of the solitonic vortex structures [27]. The parameter η_0 determines the equation of state of DM, and following the argument formulated in [19], we will put $\eta_0 \to +\infty$. The first term on the right-hand side of Eq. (1) is the kinetic term, and the second describes the interaction with the condensate gravitational potential Φ_g. The third term takes into account the bosonic self-interaction (we will consider only the case $\gamma = 2$ which corresponds to binary collisions). The fourth term accounts for the core, and the fifth term describes an isothermal envelope with effective temperature $T_{\rm eff}$ which surrounds the core. This isothermal envelope is a halo of scalar radiation, arising from the quantum interferences of excited states, which could be described as collisionless particles in classical mechanics. As a result, the envelope behaves essentially as CDM and is approximately isothermal [20]. The last term with $\xi > 0$ is a damping term and ensures that the system relaxes towards the equilibrium state.

An important feature of the Gross–Pitaevskii (GP) equation is that it satisfies the H-theorem, i.e., the free energy F of the system decreases [19]

$$\dot{F} = -\xi \int \rho \mathbf{u}^2 d\mathbf{r} \le 0,$$

where $\rho = |\psi|^2$ denotes BEC density and $\mathbf{u} = \nabla S(\mathbf{r}, t)/m$ is the velocity field. These quantities are obtained by application of the Madelung transformation, according to the expression $\psi(\mathbf{r}, t) = \sqrt{\rho(\mathbf{r}, t)} e^{iS(\mathbf{r},t)/\hbar}$, where $S(\mathbf{r}, t)$ is the phase term. The positive sign of ξ implies that the system relaxes towards the state with zero hydrodynamical velocity $\mathbf{u} = 0$. Therefore, a stationary vortex solution with nonzero $\mathbf{u}$ can be found only if we set $\xi = 0$.

The free energy $F = E - T_{\rm eff} S_B$ is expressed through the total energy E, the effective temperature $T_{\rm eff}$, and the Boltzmann entropy $S_B = -k_B \int (\rho/m)(\ln(\rho/\rho_0) - 1) d\mathbf{r}$. The total energy consists of the classical kinetic energy $\Theta_c = 1/2 \int \rho \mathbf{u}^2 d\mathbf{r}$, the quantum kinetic energy $\Theta_Q = 1/m \int \rho Q d\mathbf{r}$, the gravitational potential energy $W = 1/2 \int \rho \Phi_g d\mathbf{r}$, and the internal energy of the self-interaction $U = K \int \rho^2 d\mathbf{r}$, $E_0 = \Theta_c + \Theta_Q + W + U$. Here $Q = -\frac{\hbar^2}{2m} \frac{\Delta\sqrt{\rho}}{\sqrt{\rho}}$ is the quantum potential. A stable equilibrium state corresponds to the minimum of the free energy F at fixed total mass M of BEC. This gives the following condition of quantum hydrostatic equilibrium [19]:

$$\frac{\rho}{m}\nabla Q + \nabla P + \rho \nabla \Phi_g + \frac{\rho}{2}\nabla \mathbf{u}^2 = 0,$$

where $P = K\rho^2 + \rho \frac{k_B T_{\rm eff}}{m}$ is pressure due to the self-interaction and effective temperature. Taking into account the Poisson equation (2) and neglecting the quantum pressure term Q, we obtain the following equation of state

$$-2K\Delta\rho - \frac{k_B T_{\rm eff}}{m}\Delta \ln \rho = 4\pi G\rho + \frac{1}{2}\mathbf{u}^2, \tag{3}$$

where G is the gravitational constant. The solution of this equation is discussed in Sect. 3.

2.2 Gravitoelectromagnetic approach

To determine the gravitational field of DM halo we employ the well-known gravitoelectromagnetism (GEM) approach [38] which was previously applied to galactic structures in [34,36,37]. According to the GEM formalism, in the case of a test particle (which is luminous matter in our case) moving much slower than the speed of light c, it is convenient to represent the spacetime metric in the form

$$dS^2 = g_{\mu\nu} dx^\mu dx^\nu = \left(1 - \frac{2\Phi_g}{c^2}\right)(dx^0)^2 + \frac{4}{c^2}\left(\mathbf{A}_g \mathbf{dx}\right) dx^0 + \left(-1 - \frac{2\Phi_g}{c^2}\right)\delta_{ij} dx^i dx^j, \tag{4}$$

where Φ_g and $\mathbf{A}_g$ are the GEM scalar (gravielectric) and vector (gravimagnetic) potentials. For the gravitoelectromagnetic fields $\mathbf{E}_g$ and $\mathbf{B}_g$

$$\mathbf{E}_g = -\nabla\Phi_g - \frac{1}{2c}\partial_t \mathbf{A}_g, \tag{5}$$

$$\mathbf{B}_g = \nabla \times \mathbf{A}_g, \tag{6}$$

the Einstein equations imply the following relations:

$$\nabla \mathbf{E}_g = 4\pi G\rho,$$

$$\nabla \times \mathbf{B}_{\rm g} = \frac{2}{c}\partial_t \mathbf{E}_{\rm g} + \frac{8\pi G}{c}\mathbf{j}.$$

Here sources of the gravitational field are mass density ρ and matter current $\mathbf{j} = \rho\mathbf{u}$ ($\mathbf{u}$ is the matter velocity).

Since these equations are clearly analogous to those in the electromagnetic theory, their solutions have a form similar to Maxwell's theory

$$\Phi_{\rm g}(\mathbf{r}) = G\int_{\Omega}\frac{\rho(\mathbf{r}')d^3r'}{|\mathbf{r}-\mathbf{r}'|}, \tag{7}$$

$$\mathbf{A}_{\rm g}(\mathbf{r}) = \frac{2G}{c}\int_{\Omega}\frac{\rho(\mathbf{r}')\mathbf{u}(\mathbf{r}')d^3r'}{|\mathbf{r}-\mathbf{r}'|}, \tag{8}$$

where integration proceeds over $\mathbf{r}'$ occupied by DM particles, $\rho(\mathbf{r}')$ is the condensate density and $\mathbf{u}(\mathbf{r}')$ is the BEC velocity at $\mathbf{r}'$. Coordinates $\mathbf{r}$ are associated with the test particle, moving along geodesics in the BEC gravitational field.

Finally, the geodesic movement for a test particle, which corresponds to the spacetime metric in the GEM form,

$$\frac{d^2x^i}{dt^2} = \frac{\partial\Phi_{\rm g}}{\partial x_i} + \frac{2}{c}\frac{dA^i_{\rm g}}{dt} - \frac{2}{c}\left(\frac{\partial\mathbf{A}_{\rm g}}{\partial x_i}\frac{d\mathbf{x}}{dt}\right)$$

can be equivalently described as the classical motion $m\ddot{\mathbf{x}} = \mathbf{F}_{\rm g}$ where the gravitoelectromagnetic analog of the Lorentz force

$$\mathbf{F}_{\rm g} = -m\left(\mathbf{E}_{\rm g} + \frac{2}{c}\mathbf{v}\times\mathbf{B}_{\rm g}\right) = m(\mathbf{a}_{\rm E} + \mathbf{a}_{\rm B}), \tag{9}$$

$\mathbf{v}$ is the particle velocity and m is its mass. Here we introduced gravielectric $\mathbf{a}_{\rm E} = -\mathbf{E}_{\rm g}$ and gravimagnetic $\mathbf{a}_{\rm B} = -\frac{2}{c}\mathbf{v}\times\mathbf{B}_{\rm g}$ components of acceleration.

3 Halo density profile

The model, based on the generalized GPP equations (see Eqs. (1), (2)) describes the core-envelope structure of DM halo with a dense core and diffuse isothermal envelope. The model yields the following equation of state for the ULDM $P = K\rho^2 + \rho\frac{k_B T_{\rm eff}}{m}$ (see Sect. 2). Thus, one can conclude, that in the core region equation of state is approximately $P = K\rho^2$, because the weak self-interaction dominates over effective temperature impact due to large density. This is why the latter will be neglected in the discussion of the core states. On the contrary, in the isothermal envelope region, we have the equation of state $P = \rho\frac{k_B T_{\rm eff}}{m}$, which means that the effective temperature term plays a crucial role there.

Based on these considerations, we calculate the halo density in two steps. Firstly, we reproduce the numerical result for the total density of the non-rotating halo (see the original result in [19]), which defines density distribution in the isothermal envelope region. This step is needed as a starting point to define isothermal envelope density distribution and to compare the discussed in [19] $s = 0$ solitonic core with the new case of vortex core $s = 1$. Secondly, under the assumption that core and envelope do not interact, we discuss the core density profile separately by means of variational ansatz [25]. This way we will study the spherically symmetric ($s = 0$) and the single-charged vortex ($s = 1$) solutions for the core density distribution.

3.1 Isothermal envelope

In the first case of a non-rotating core, we can set $\mathbf{u} = 0$, and then the Eq. (3) simplifies

$$-\frac{4\pi a_s\hbar^2}{m^3}\Delta\rho - \frac{k_B T_{\rm eff}}{m}\Delta\ln\rho = 4\pi G\rho,$$

where we took into account that $K = \frac{4\pi a_s\hbar^2}{m^3}$.

It is convenient to introduce the density function and the radial coordinate $\rho = \rho_0 e^{-f}$, $y = r/r_0$, where

$$r_0 = \sqrt{\frac{k_B T_{\rm eff}}{4\pi G\rho_0 m}} \tag{10}$$

and ρ_0 defines the density at the center. The equation of state can be rewritten in the following form:

$$\frac{d^2f}{dy^2} + \frac{2}{y}\frac{df}{dy} = \frac{\chi\left(\frac{df}{dy}\right)^2 + 1}{\chi + e^f}, \tag{11}$$

where $\chi = 4\pi a_s\hbar^2\rho_0/(m^2 k_B T_{\rm eff})$. The boundary conditions are $f(0) = 0$ and $\frac{df}{dy}(0) = 0$, which define the boundary conditions for the density function $\rho_0 = \rho(0)$ and $\frac{d\rho(0)}{dr} = 0$. We solve Eq. (11) numerically for different values of χ and present solutions in Fig. 1a. The isothermal envelope density distribution is defined as $\rho = \rho_0 e^{-f} = \rho_0 f_{\rm N}(r)$, where f is a numerical solution of Eq. (11).

The profile has a solitonic core and an isothermal envelope whose density decreases as $\rho(r) \sim k_B T_{\rm eff}/(2\pi G m r^2) = v_\infty^2/(4\pi G r^2)$ [19] in agreement with observations (here v_∞ is the constant rotational velocity in the large distance limit). Thus, we see that the existence of the core-envelope structure is essential to describe observations that could not be achieved with the standard system of the GPP equations (they predict only the compact core with exponentially decaying density). The existence of a BEC core in the ULDM model was also discussed in [21–24].

The possible physical origin of the core-envelope structure could be the merger of two-state configurations when the total system tends to a virialized state, and the obtained averaged profile has a core and a tail structure [44]. The process of

halo formation usually undergoes gravitational cooling [45], which is discussed in [45,46]. Gravitational cooling process for initially quite arbitrary density profiles leads to relaxation and virialization through the emission of scalar field particles [47]. The resulting profile has the same dense core and diffuse envelope structure.

In the case $s = 1$, the hydrodynamical velocity $\mathbf{u}$ does not vanish in the inner region due to the existence of the vortex. The definition of the velocity profile in the isothermal halo region is a complicated task. One would expect that there is an intermediate region between the core and isothermal envelope, where the hydrodynamical velocity is small but nonzero, and at large enough distances, we should have $\mathbf{u} = 0$. This is due to the divergent mass of the isothermal envelope, which therefore cannot rotate in order for kinetic energy to be finite. For an estimate, we simply put $\mathbf{u} = 0$ in the whole isothermal envelope region. This approximation can be justified by the negligibly small density of the isothermal envelope in comparison with the core density, so its rotation would have no sufficient impact on the system. Hence the density profile in the envelope region remains unchanged. Thus, to define isothermal envelope density distribution we use the numerical solution for $\rho = \rho_0 f_{\rm N}(r)$, obtained earlier in the case of non-rotating core. The density profile in the core region will be discussed in the next section in detail.

To reproduce the Milky Way halo mass $M = 1.3 \times 10^{12} M_\odot$ and radius $R_{\rm halo} = 287$ kpc [48], taking into account the model described in [19], we choose the following values of the particle mass $m = 2.92 \times 10^{-22}$ eV/c^2 $= 0.52 \times 10^{-57}$ kg, scattering length $a_{\rm s} = 8.17 \times 10^{-77}$ m, effective DM temperature $T_{\rm eff} = 5.09 \times 10^{-25}$ K, central density in the spherical case $\rho_0 = 0.34 \times 10^{-17}$ kg/m^3, distance scaling parameter $r_0 = 0.071$ kpc and $\chi = 20$. For the spherically symmetric case, the chosen parameters yield the core with mass $M_{\rm c} = 6.39 \times 10^{10} M_\odot$ and radius $R_{\rm c} = 1$ kpc.

The BEC temperature of such ultralight bosons can be estimated in the framework of a simple model of non-interacting bosonic particles. This temperature (see, e.g. [17,18]) appears to be much higher than the effective temperature, and therefore thermal excitations can be neglected. However, the interactions, especially the dominating self-gravitating component, could significantly change the value of the temperature. To the best of our knowledge, a rigorous derivation of the critical temperature for self-gravitating bosonic DM has not yet been discussed in the literature, although it is important and should be addressed in future.

3.2 Core stationary states

The dynamics of self-gravitating BEC of N weakly interacting bosons with mass m is described by the GPP system of equations with the term, corresponding to the effective temperature impact:

$$i\hbar\frac{\partial\psi}{\partial t} = \left(-\frac{\hbar^2}{2m}\nabla^2 + gN|\psi|^2 + m\Phi_g + 2k_B T_{\rm eff}\ln\left|\frac{\psi}{\psi_0}\right|\right)\psi \tag{12}$$

$$\nabla^2\Phi_g = 4\pi G m N|\psi|^2 \tag{13}$$

where $g = \frac{4\pi\hbar^2 a_s}{m}$ is the coupling strength that corresponds to the two-particle interaction, a_s is the s-wave scattering length, $\Phi_{\rm g}$ is the gravitational potential and G is gravitational constant.

The GPP system of Eqs. (12) and (13) includes three crucial physical parameters: particle mass m, the total number of particles N (or, equivalently, total mass M) and coupling strength g (or, equivalently, self-interaction constant $\frac{\lambda}{8\pi} = \frac{a_{\rm s}}{\lambda_{\rm c}}$, where $\lambda_{\rm c} = \frac{\hbar}{mc}$ is the Compton wavelength of bosons) [25].

The GPP system of equations is invariant under the transformation $t = \lambda_*^2 t'$, $\mathbf{r} = \lambda_* \mathbf{r}'$, $\psi = \lambda_*^{-2}\psi'$, $\Phi_{\rm g} = \lambda_*^{-2}\Phi_{\rm g}'$, $g = \lambda_*^2 g'$, where $\lambda_* > 0$, which allows us to scale-out the coupling constant to $g = 1$.

In order to simplify calculations, it is convenient to introduce dimensionless variables and wave function

$$i\frac{\partial\psi}{\partial t} = \left(-\frac{1}{2}\nabla^2 + |\psi|^2 + \Phi_{\rm g} + \tilde{T}_{\rm eff}\ln|\psi|\right)\psi, \tag{14}$$

$$\nabla^2\Phi_{\rm g} = |\psi|^2, \tag{15}$$

where the dimensional variables are related to the dimensionless ones as follows: $\mathbf{r} = \mathbf{r}_{\rm ph} L$, $t = \omega_* t_{\rm ph}$, $\Phi_{\rm g} = \left(\frac{L}{\lambda_{\rm c}}\right)^2 \frac{\Phi_{\rm gph}}{c^2}$, and $\psi = \frac{\lambda}{8\pi}\left(\frac{m_{\rm Pl}}{m}\right)^2 \sqrt{4\pi G M}\frac{\hbar}{mc^2}\psi_{\rm ph}$. Here the distance and time scaling parameters are $L = \lambda_{\rm c}\frac{m_{\rm Pl}}{m}\sqrt{\frac{\lambda}{8\pi}} = \frac{m_{\rm Pl}\hbar}{m^2 c}\sqrt{\frac{\lambda}{8\pi}} = 0.99 \times 10^{19} m = 0.32$ kpc and $\omega_* = \frac{c\lambda_{\rm c}}{L^2} = 2.08 \times 10^{-15}$ s^{-1}. The dimensionless effective temperature parameter is $\tilde{T}_{\rm eff} = \frac{2k_{\rm B}T_{\rm eff}}{\omega_*\hbar}$ and will be neglected in the following discussion because the corresponding term $\tilde{T}_{\rm eff}\ln|\psi|$ is negligibly small in the core region. Therefore, we neglect the temperature effects in the analysis of the BEC core density distribution.

For the BEC core mass $M_{\rm c} = 6.39 \times 10^{10} M_\odot$ and radius $R_{\rm c} = 1$ kpc, we solve the GPP Eqs. (14) and (15) by using the variational ansatz in cylindrical coordinates r, z and ϕ

$$\psi(r,\phi,z) = A\left(\frac{r}{R}\right)^s e^{-\frac{r^2}{2R^2} - \frac{z^2}{2(R\eta)^2} + is\phi}. \tag{16}$$

Here R and η are variational parameters, which will be fixed later. Constant A is fixed by the normalization condition

$$A = \sqrt{\frac{N_0}{\pi^{3/2}\eta R^3 s!}}, \tag{17}$$

the cases $s = 0, 1$ are considered, and N_0 is defined by the core mass

$$N_0 = 4\pi \frac{M_c}{m_{Pl}} \sqrt{\frac{\lambda}{8\pi}} = 2.55 \cdot 10^4,$$

where $m_{Pl} = \sqrt{\frac{\hbar c}{G}}$ is the Planck mass and $\lambda/(8\pi) = 1.21 \times 10^{-91}$ is the self-interaction coupling constant.

The dimensionless quantities and the physically observed ones are related as follows:

$$R_c = R_{99} L = \frac{m_{Pl}\hbar}{m^2 c} \sqrt{\frac{\lambda}{8\pi}} R_{99}, \tag{18}$$

$$\rho = M|\psi_{ph}|^2 = \frac{M}{L^3 N_0}|\psi|^2 = \rho_0 \left(\frac{r}{R}\right)^{2s} e^{-\frac{r^2}{R^2} - \frac{z^2}{(R\eta)^2}}, \tag{19}$$

where R_{99} is the dimensionless radius which contains 99 percent of the mass of the core (the variational analysis gives $R_{99} \approx 2.38R$ in the case of solitonic core and $R_{99} \approx 2.58R$ in the case of vortex core), ρ is the condensate density, and $\rho_0 = MA^2/(L^3 N_0)$ is the density scaling parameter. R_c denotes the total radius of the core in physical units.

Using the variational ansatz for the BEC wave function (16), we obtain the energy [25]:

$$E = \int d^3\mathbf{r}\psi^*(\mathbf{r},t)\left(-\frac{1}{2}\nabla^2 + |\psi|^2 + \Phi_g\right)\psi(\mathbf{r},t)$$
$$= \epsilon\left(\frac{N_0(1+2\eta^2(1+s))}{4R^2\eta^2} + \frac{N_0^2\Gamma(s+1/2)}{4\sqrt{2}\pi^2 R^3 \eta \Gamma(s+1)} - \frac{N_0^2}{8\pi R}\int_0^\infty \mathrm{Erfc}\left(\frac{k_*\eta}{\sqrt{2}}\right) L_s^2\left(\frac{k_*^2}{4}\right) e^{-\frac{k_*^2(1-\eta^2)}{2}} dk_*\right) \tag{20}$$

where $\Gamma(x)$ denotes the Gamma function, $\mathrm{Erfc}(x)$ is the complementary error function and $L_s(x)$ is a Laguerre polynomial. Here $\epsilon = (\hbar^2/4\pi m_{Pl}\lambda_c^2)(8\pi/\lambda)^{3/2}$ is characteristic energy, which does not depend on variational parameters.

In what follows, we will use $r_0 = 2.18 \times 10^{18}$ m $= 0.071$ kpc $= 0.22$ L as the distance scaling parameter.

In the subsection below, we investigate the case $s = 0$.

3.2.1 Non-rotating spherically-symmetric core

In this case, the BEC wave function in Eq. (16) depends only on radial distance r in spherical coordinates

$$\psi(r) = Ae^{-\frac{r^2}{2R^2}} \tag{21}$$

and the density function (see Eq. (19)) equals

$$\rho(r) = \rho_0 e^{-\frac{r^2}{R^2}}. \tag{22}$$

In what follows, r will denote spherical distance, when the $s = 0$ case is discussed.

We should relate R and the BEC core radius R_c which is defined through $M_c = \frac{4}{\pi}\rho_0 R_c^3$ [25]. Since $\rho_0 = M_c A^2/(L^3 N_0)$, the numerical result for halo density (see Fig. 1a) gives $\frac{R_c}{LR} = 1.64$ or $R = 8.66$ in the r_0 scale. It is interesting to compare the obtained R with its value in the variational analysis method used in [25]. Substituting $\eta = 1$ and $s = 0$ in the energy functional in Eq. (20), we get

$$\frac{E}{\epsilon} = \frac{3N_0}{4R^2} + \frac{N_0^2}{4\sqrt{2}\pi^{3/2}R^3} - \frac{N_0^2}{8\pi R}\int_0^\infty \mathrm{Erfc}\left(\frac{k_*}{\sqrt{2}}\right) dk_*.$$

Its extremum is defined by the equation

$$R^2 - \frac{6\sqrt{2}\pi^{3/2}}{N_0} R - 3 = 0 \tag{23}$$

that gives $R = 1.73$ or $R = 7.86$ in the r_0 scale. Thus, $R_c = 0.9$ kpc (see Eq. (18)) and, therefore, the variational analysis method and numerical calculation (see Fig. 1a) are in a good agreement.

3.2.2 Rotating axially-symmetric core

In the case $s = 1$ (see Eq. (16)), we have a wave function, which depends on cylindrical coordinates r, z, ϕ

$$\psi(r,\phi,z) = A\frac{r}{R}e^{-\frac{r^2}{2R^2} - \frac{z^2}{2(R\eta)^2} + i\phi} \tag{24}$$

and the density function equals

$$\rho(r,z) = \rho_0 \left(\frac{r}{R}\right)^2 e^{-\frac{r^2}{R^2} - \frac{z^2}{(R\eta)^2}}, \tag{25}$$

where A is given by Eq. (17).

The dimensionless total energy in Eq. (20) for $s = 1$ reads

$$\frac{E}{\epsilon} = \frac{N_0(1+4\eta^2)}{4R^2\eta^2} + \frac{N_0^2}{8\sqrt{2}\pi^{3/2}R^3\eta} - \frac{N_0^2}{8\pi R}\int_0^\infty \mathrm{Erfc}\left(\frac{k_*\eta}{\sqrt{2}}\right)\left(1 - \frac{k_*^2}{4}\right)^2 e^{-\frac{k_*^2(1-\eta^2)}{2}} dk_*.$$

Equations of an extremum of the total energy with respect to η and R yield the solution $\eta = 1.464$, and $R = 1.226$ in the L scale. In the r_0 scale, we have $R = 5.57$. To determine the core density distribution, we use the variational

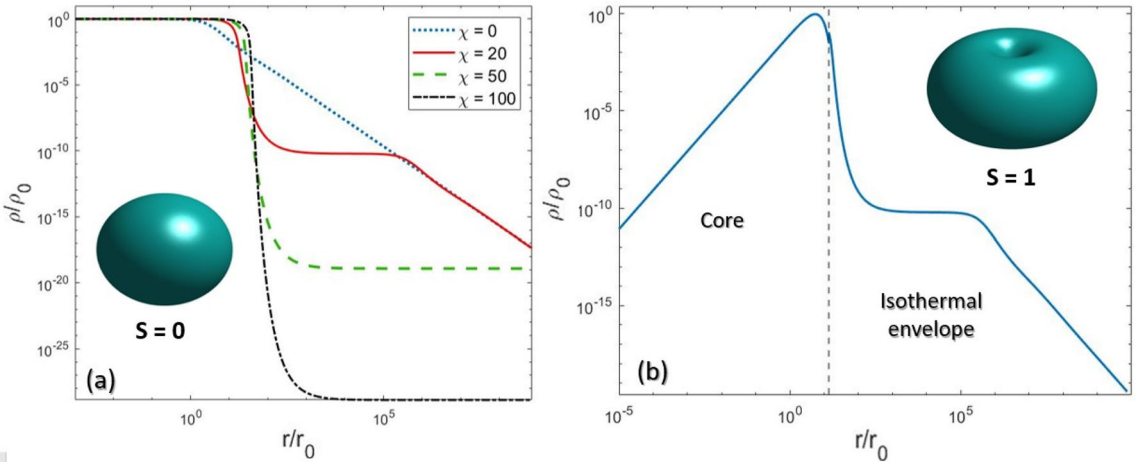

Fig. 1 Halo density profile ρ/ρ_0 as a function of dimensionless r/r_0 coordinate in the plane $z = 0$, both x and y axes have log scale. The cyan insets in both plots show 3D density isosurfaces of the corresponding BEC cores. Left panel (**a**) shows the halo with the BEC core in a soliton state ($s = 0$). Three curves correspond to different values of parameter $\chi = 4\pi a_s \hbar^2 \rho_0/(m^2 k_B T_{\text{eff}})$, so that while increasing χ one decreases effective temperature T and vice versa. Right panel (**b**) shows the halo with the core in a vortex state ($s = 1$, $\chi = 20$). Note, we investigate in detail the isothermal envelope for $\chi = 20$, which is consistent with observations for the Milky Way. The black dashed line divides the distribution into two parts: the inner region with a rotating core and the outer region composed of an isothermal envelope

analysis result. We assume that the core interacts negligibly weakly with the isothermal envelope. Therefore, for the isothermal envelope region, we use the numerical distribution $f_{\text{N}}(r_{\text{sph}}) = f_{\text{N}}(\sqrt{r^2+z^2})$ (see Fig. 1a), derived under $\mathbf{u} = 0$ condition.

Thus, we obtain (see Fig. 1b)

$$\rho(r,z) = \rho_0 \begin{cases} 2.6\left(\frac{r}{R}\right)^2 e^{-\frac{r^2}{R^2}-\frac{z^2}{(R\eta)^2}}, r_{\text{sph}} \le R_{\text{c}} \\ f_{\text{N}}\left(r_{\text{sph}}\right), r_{\text{sph}} > R_{\text{c}}, \end{cases} \tag{26}$$

where $r = \sqrt{x^2+y^2}$ and z are cylindrical coordinates and $r_{\text{sph}} = \sqrt{x^2+y^2+z^2}$. Here ρ_0 is the spherical halo central density. The spherically symmetric isothermal envelope density $\rho(r,z) = \rho_0 f_{\text{N}}\left(r_{\text{sph}}\right)$ is found numerically by solving Eq. (11). The total core radius R_{c} is defined by Eq. (18).

By using $\mathbf{u} = \frac{\mathbf{j}_{\text{ph}}}{\rho}$ and the particle current

$$\begin{aligned} \mathbf{j}_{\text{ph}} &= -\frac{i\hbar}{2m}(\psi^*_{\text{ph}}\nabla\psi_{\text{ph}} - \psi_{\text{ph}}\nabla\psi^*_{\text{ph}}) \\ &= \frac{\hbar}{m}\frac{|\psi_{\text{ph}}|^2}{r}\mathbf{e}_\phi, \end{aligned}$$

we find the velocity distribution $\mathbf{u}(\mathbf{r})$ of DM particles

$$\mathbf{u} = \frac{\frac{\hbar}{m}\frac{|\psi_{\text{ph}}|^2}{r}}{|\psi_{\text{ph}}|^2}\mathbf{e}_\phi = \frac{\hbar}{m}\frac{1}{r}\mathbf{e}_\phi = \alpha\frac{cr_0}{r}\mathbf{e}_\phi, \tag{27}$$

where $\alpha = \hbar/(mr_0c) = 0.31 \cdot 10^{-3}$. Obviously, the velocity of condensate particles increases while approaching the center of the vortex. Note that there is an inner region where the velocity becomes of the order of c and, therefore, this region cannot be described by making use of the gravitoelectromagnetism ansatz (see Appendix A for explanation). This region is limited by the radial distance $r = \alpha r_0 = 2.2 \times 10^{-5}$ kpc.

In the two following sections, by using the formalism of GEM, we describe particle movement in the gravitational field of DM in the $s = 0, 1$ states aiming to understand how baryonic matter particles interact with the proposed DM.

4 Gravielectric field and rotation curves

In this section, we obtain numerical results for the gravielectric (Newtonian) component of the DM halo gravitational field. Having calculated the field, we analyze the rotation curves, predicted by the model in the cases of soliton and vortex core.

To determine the gravielectric potential in the case of a non-rotating halo we use the numerically obtained density distribution (see Fig. 1a). In the case of a rotating axially symmetric halo, the mass density distribution is shown in Fig. 1b.

In the spherically symmetric case of non-rotating halo ($s = 0$), only the radial component of the gravielectric field is not zero (see Eq. (7)) and the corresponding gravielectric acceleration $\mathbf{a}_{\text{E}} = -\mathbf{E}_{\text{g}} = a_{\text{E}}\mathbf{e}_r$ (see Eq. (9)) is presented in Fig. 2. The acceleration at large distances behaves like $a_{\text{E}}/a_0 = 82.66 r_0/r$, i.e., $a_{\text{E}} = 9.3 \times 10^{-29} \frac{\text{kpc}^2}{s^2} \times 1/r$. Here $a_0 = G\rho_0 r_0 = 5.38 \times 10^{-13}$ km/s^2. In the core region, where the density distribution is described by the variational

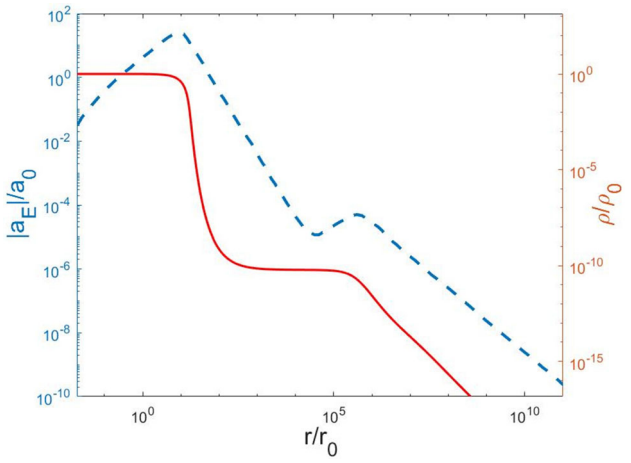

Fig. 2 The radial component of gravielectric field a_E/a_0 (blue dashed line) and density (red solid line) of the non-rotating halo ($s = 0$ core) as functions of the dimensionless r/r_0 coordinate, both x and y axes have log scale. Here $a_0 = 5.38 \times 10^{-13}$ km/s^2, $r_0 = 71$ pc

ansatz (22), the gravielectric potential and the corresponding acceleration can be found analytically

$$\frac{1}{r^2}\frac{\partial}{\partial r}r^2\frac{\partial}{\partial r}\Phi_g = -4\pi G\rho_0 e^{-\frac{r^2}{R^2}}.$$

The general solution is given by

$$\Phi_g(a) = -4\pi G\rho_0 R^2\left(\frac{c_1}{r} + c_2 - \frac{R\sqrt{\pi}\,\mathrm{Erf}(r/R)}{4r}\right).$$

where $\mathrm{Erf}(x)$ denotes the error function and c_1, c_2 are constants.

We can set $c_2 = 0$. At a large distance, the gravielectric potential of the halo must be equal to the potential of a body with the same mass $M = \pi^{3/2}\rho_0 R^3$. This implies that $c_1 = 0$. Thus, $\Phi_g(r)$ is completely determined and we have the radial acceleration

$$\mathbf{a}_E(r) = \nabla\Phi_g(r)$$
$$= \pi G\rho_0 R^3\left(\frac{2e^{-r^2/R^2}}{Rr} - \frac{\sqrt{\pi}\,\mathrm{Erf}\left(\frac{r}{R}\right)}{r^2}\right)\mathbf{e}_r.$$

Clearly, a_E has a maximum at $r = R = 8.66$ in the r_0 scale in agreement with the radial gravielectric acceleration shown in Fig. 2.

Gravielectric field in the case of vortex core has radial and z components in cylindrical coordinates, namely, $\mathbf{a}_E = a_{Er}\mathbf{e}_r + a_{Ez}\mathbf{e}_z$. They are illustrated in Figs. 3 and 4, respectively. The radial dependence of the gravielectric radial acceleration in the $z = 0$ plane is shown in Fig. 5. Notice that at $r \approx 3r_0 = 0.2$ kpc the acceleration changes sign, hence test particles are repelled in the interior region and attracted in the exterior region. This result stems from the geometry of the considered doughnut-shaped halo with a hole.

Now we aim to determine the impact of the gravitational field of the DM halo on the movement of celestial bodies in the Milky Way galaxy. According to our model (see Sect. 3) density distribution depends on the state of the core, which must lead to a difference between the rotation curves, which they induce. To demonstrate how the gravielectric acceleration induces rotation in the $s = 0$ and $s = 1$ cases, we present the rotation velocity v in the $z = 0$ plane as a function of the radial distance r in Fig. 6. The new result here is the curve in the case $s = 1$, while $s = 0$ case was discussed earlier in [19]. Remarkably, rotation curves in the internal region are significantly affected by the topology of the BEC core.

The two halos with $s = 0$ and $s = 1$ core have equal mass, which is the observed mass of DM halo in the Milky Way, according to the model discussed in Sect. 3. The numerical results indeed show that at large distances the corresponding

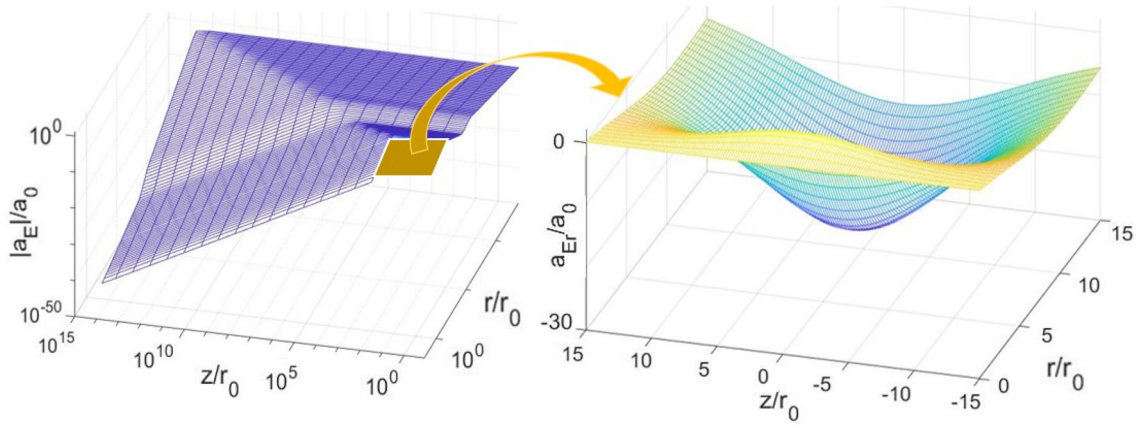

Fig. 3 The radial component of gravielectric acceleration a_{Er}/a_0 induced by the rotating halo ($s = 1$ core) as a function of dimensionless r/r_0 and z/r_0 coordinates. Here $a_0 = 5.38 \times 10^{-13}$ km/s^2, $r_0 = 71$ pc. The left panel shows the isothermal envelope region with the three axes in the log scale and the right panel is a zoom-in of the core region

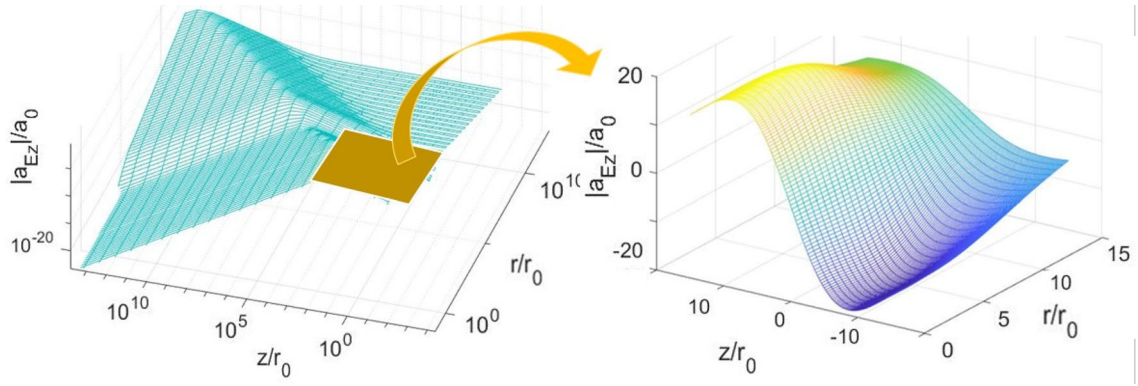

Fig. 4 The z-component of gravielectric acceleration $a_{\mathrm{E}z}/a_0$ induced by the rotating halo ($s = 1$ core) as a function of dimensionless r/r_0 and z/r_0 coordinates. Here $a_0 = 5.38 \times 10^{-13}$ km/s^2, $r_0 = 71$ pc. The left panel shows the isothermal envelope region with the three axes in the log scale and the right panel is a zoom-in of the core region

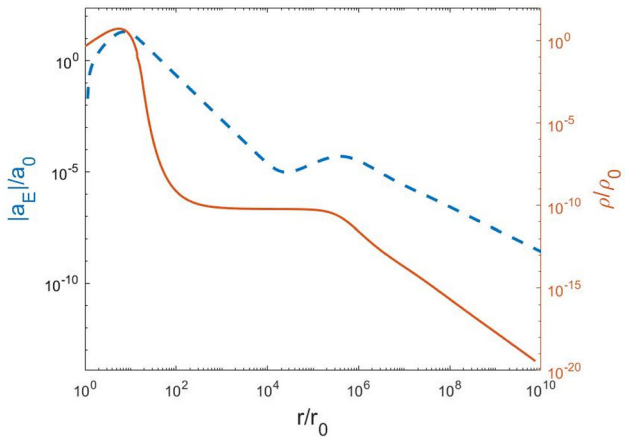

Fig. 5 The radial component of gravielectric acceleration $a_{\mathrm{E}r}/a_0$ (blue dashed line) and density (red line) of the rotating halo ($s = 1$ core) as functions of dimensionless r/r_0 coordinate in the $z = 0$ plane, both x and y axes have log scale. Here $a_0 = 5.38 \times 10^{-13}$ km/s^2, $r_0 = 71$ pc

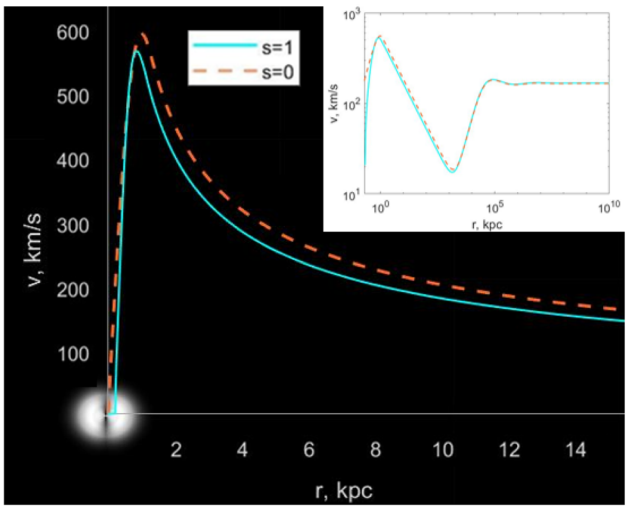

Fig. 6 The rotation (Kepler) velocity v in the $z = 0$ plane as a function of the radial distance r. The pink dashed line corresponds to the non-rotating spherical halo ($s = 0$ core) and the cyan solid line to the rotating halo ($s = 1$ core). The background represents a gradient plot of the density distribution in $s = 1$ case. The inset shows rotational curves in the log-log scale for a wide range of radial distances

rotational curves have the same asymptotic. Note that, the gravielectric force in $s = 1$ case changes its sign at $r = 3r_0 = 0.2$ kpc. Hence, at distances less than 0.058 kpc there are no stable rotation orbits in the rotating halo model. However, the stable orbits are possible if one includes not only DM but also the other sources of the gravitational field, namely, the baryonic galactic bulge and the supermassive black hole in the central region of the galaxy.

Note that rotation curves exhibit a pronounced minimum at $r \approx 10^3$ kpc (see inset in Fig. 6). Such a non-monotonic behaviour of the rotation curves was pointed out in Ref. [19]. As was pointed out in Ref. [19] this local minimum crucially depends on parameter $\chi = 4\pi a_{\mathrm{s}}\hbar^2\rho_0/(m^2 k_{\mathrm{B}} T_{\mathrm{eff}})$. To compare obtained rotational curves with observations one needs also to account for baryonic matter distribution. However, the lack of reliable observational data for the rotational curve of the Milky Way at distances much greater 15 kpc (see e.g. [49]) does not allow one to verify these theoretical predictions at large distances.

5 Gravimagnetic field in the BEC core

In this section, we obtain numerical results for the gravimagnetic (first post-Newtonian) component of the DM halo gravitational field (see Sect. 2.2 of Sect. 2). The component is induced by a moving source, hence, it is nonzero only in the second case of the DM halo with a vortex core.

To determine the gravimagnetic potential in the case of a rotating axially symmetric halo we use the mass density and

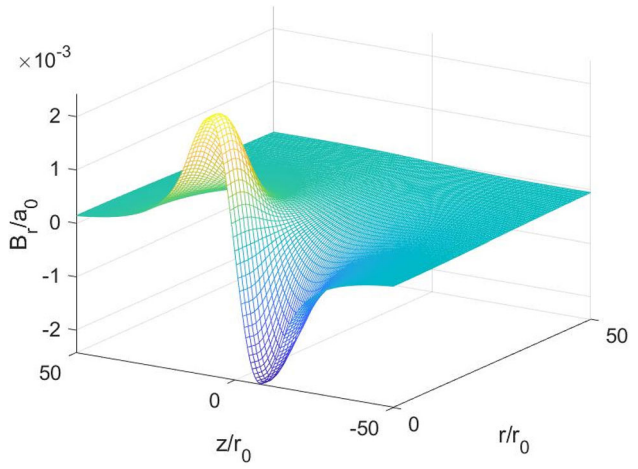

Fig. 7 The radial component of gravimagnetic field B_r/a_0 induced by the rotating core as a function of dimensionless r/r_0 and z/r_0 coordinates. Here $a_0 = 5.38 \times 10^{-13}$ km/s^2, $r_0 = 71$ pc

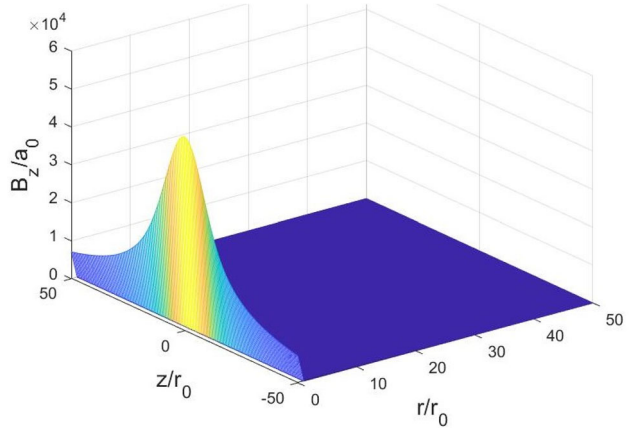

Fig. 8 The z-component of gravimagnetic field B_z/a_0 induced by the rotating core as a function of dimensionless r/r_0 and z/r_0 coordinates. Here $a_0 = 5.38 \times 10^{-13}$ km/s^2, $r_0 = 71$ pc

velocity distributions given by Eqs. (26) and (27). The calculation is based on Eqs. (8) and (6). The results of numerical integration for radial and z-components of the gravimagnetic field, $\mathbf{B} = B_r\mathbf{e}_r + B_z\mathbf{e}_z$, are shown in Figs. 7 and 8, respectively. Figure 9 displays the z-component of the gravimagnetic field B_z in the $z = 0$ plane (the radial component of the gravimagnetic field equals zero in this plane).

Having determined the gravimagnetic field, we can calculate the corresponding acceleration of a test particle. Using Eq. (9), we have

$$\begin{aligned}\mathbf{a}_{\mathrm{B}}(\mathbf{r} = (a, b, k)) &= -\frac{2}{c}v\mathbf{e}_\phi \times \mathbf{B}_{\mathrm{g}} \\ &= -0.34\alpha G\rho_0 r_0 \frac{v}{c}(B_z(a, b, k)\mathbf{e}_r + B_r(a, b, k)\mathbf{e}_z) \\ &= a_{\mathrm{Br}}(a, b, k)\mathbf{e}_r + a_{\mathrm{Bz}}(a, b, k)\mathbf{e}_z.\end{aligned}$$

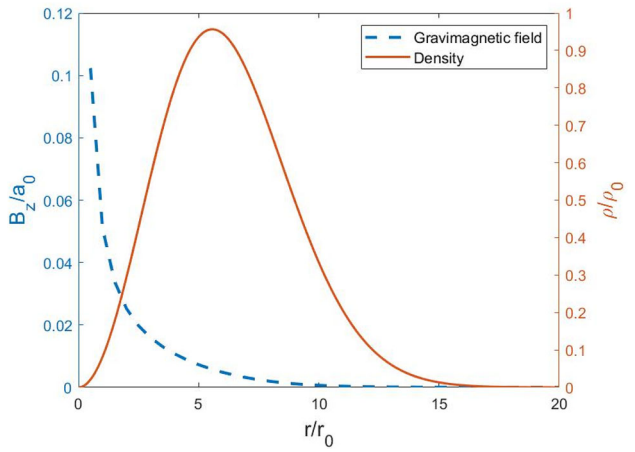

Fig. 9 The z-component of the gravimagnetic field B_z/a_0 (blue dashed line) and density (red line) of the rotating core as functions of dimensionless r/r_0 in $z = 0$ plane. Here $a_0 = 5.38 \times 10^{-13}$ km/s^2, $r_0 = 71$ pc

Table 1 Parameters of the Milky Way's rotational velocity profiles [50]

Galactic disk	v_1 (km/s)	γ_0 km/s kpc	γ_1 km/s kpc
Thin disk	236.71	45.41	− 1.93
Thick disk	206.93	39.086	− 2.30

where $a = r/r_0$, $b = \phi$, $c = z/r_0$ are rescaled cylindrical coordinates.

This allows us to estimate the impact of the gravimagnetic field on stars' motion. In the case of the Milky Way galaxy, $v = v_0 + \gamma_0 r_0 a$ if $a < a_{\mathrm{break}}$ and $v = v_1 + \gamma_1 r_0 a$ for $a \geq a_{\mathrm{break}}$ [50]. Constants γ_0, γ_1, a_{break}, and v_1 are different for the thick and thin galactic disks' velocity profiles. Setting $R_{\mathrm{break}} = r_0 a_{\mathrm{break}} = 5$ kpc and v_0=0 in both cases gives the values of parameters presented in Table 1. This approximation is valid up to 13 kpc $= 180 r_0$ [50]. We should emphasize here that v includes only the component of velocity directed along $\mathbf{e}_\phi$ and does not include the component along $\mathbf{e}_r$. It is important to distinguish the ϕ-component and the absolute value of the whole velocity when dealing with sufficiently non-circular elliptic orbits.

According to Eq. (9), the gravimagnetic acceleration in galactic plane $c = 0$ can be estimated as

$$\mathbf{a}_{\mathrm{B}} = -0.34\alpha G\rho_0 r_0 \frac{v_i + \gamma_i r_0 a}{c} B_z(a, b, 0)\mathbf{e}_r,$$

where $i = 0$ for $a < a_{\mathrm{break}}$ and $i = 1$ for $a \geq a_{\mathrm{break}}$. The corresponding plot is shown in Fig. 10. The spike on the red curve, which shows the modulus of the ratio of the gravimagnetic acceleration to the gravielectric one $|a_{\mathrm{Br}}/a_{\mathrm{Er}}|$ appears because the gravielectric acceleration changes sign at $r = 3r_0 = 0.2$ kpc.

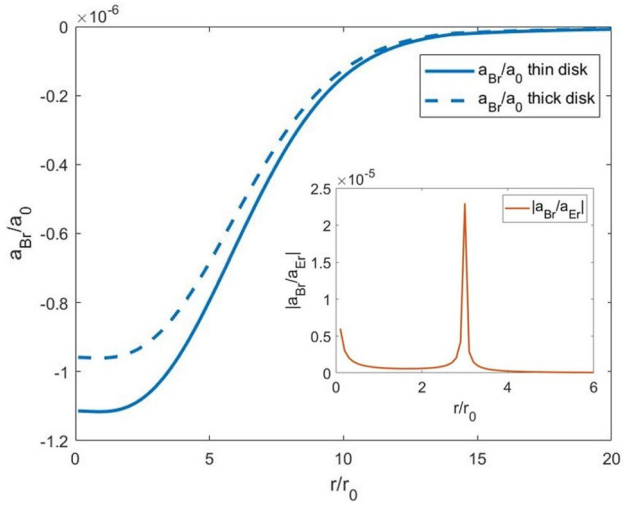

Fig. 10 The radial component of gravimagnetic acceleration (solid and dashed blue lines) $a_{\rm Br}/a_0$ for thin and thick disks, respectively, and the absolute value of the ratio of gravimagnetic to gravielectric accelerations $|a_{\rm Br}/a_{\rm Er}|$ (both for thin and for thick disks) as a function of r/r_0. Here $a_0 = 5.38 \times 10^{-13}$ km/s^2, $r_0 = 71$ pc

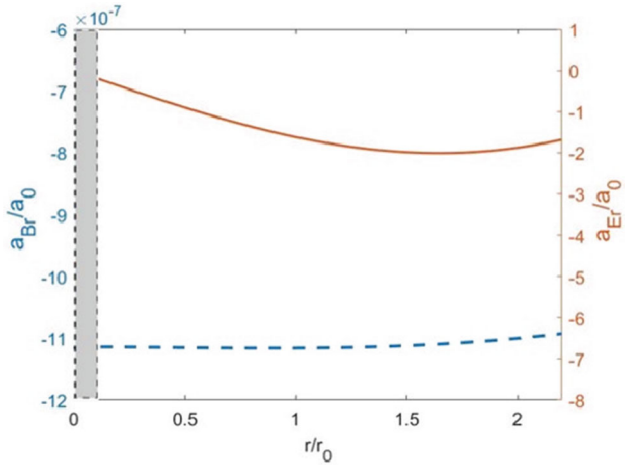

Fig. 11 The radial component of gravimagnetic acceleration (dashed blue line) $a_{\rm Br}/a_0$ and gravielectric acceleration (red line) $a_{\rm Er}/a_0$ in the inner region of halo. Here the gray region corresponds to $r < 0.1r_0$, where the gravimagnetic approximation is not valid. Here $a_0 = 5.38 \times 10^{-13}$ km/s^2, $r_0 = 71$ pc

It is interesting that $a_{\rm Br}(a)$ tends to a constant in the $a \ll 1$ limit (see Fig. 11). This directly follows from the analytical expression. In the interior region $r < 5$ kpc, we have

$$\frac{a_{\rm Br}}{a_0} = -0.34\alpha \frac{\gamma_0 r_0 a}{c} B_z(a, b, 0).$$

In the $a \ll 1$ limit, we find

$$B_z(a, b, 0) \approx \frac{2\pi}{a} \int_0^\infty dx \int_{-\infty}^\infty dz \frac{x^2}{\sqrt{x^2+z^2}} e^{-\frac{x^2}{R^2} - \frac{z^2}{(R\eta)^2}}.$$

The last integral can be calculated numerically which yields

$$\frac{a_{\rm Br}}{a_0} \approx -0.34\alpha \frac{\gamma_0 r_0}{c} \times 10^3 = 10^{-6}.$$

We see that in the case under consideration, the gravimagnetic acceleration indeed tends to a constant in the $a \ll 1$ limit.

The gravimagnetic field calculations performed in this section allow us to obtain some testable predictions of the model. According to numerical results for $\mathbf{B}_{\rm g}$ and $\mathbf{E}_{\rm g}$, the gravielectric force changes its sign at $r = 3r_0 = 0.2$ kpc, and the gravimagnetic force component is attractive or repulsive, depending on the direction of the motion. The acceleration in the polar coordinates (r, ϕ) is given by $\mathbf{a} = (\ddot{r} - r\dot{\phi}^2)\mathbf{e}_r + (r\ddot{\phi} + 2\dot{r}\dot{\phi})\mathbf{e}_\phi$. Then the equations of motion for a star take the form

$$\frac{d^2r}{dt^2} = r\left(\frac{d\phi}{dt}\right)^2 - E_r - \frac{2B_z r}{c}\frac{d\phi}{dt}, \tag{28}$$

$$r\frac{d^2\phi}{dt^2} = \frac{2B_z}{c}\frac{dr}{dt} - 2\frac{dr}{dt}\frac{d\phi}{dt}. \tag{29}$$

Since the gravielectric acceleration dominates over the gravimagnetic one, it suffices to take the latter into account as a perturbation. Therefore, we treat $B_{\rm g}$ as the first-order perturbation and expand $\phi(t)$ and $r(t)$ around the solution $r_{\rm c}$ and $\phi_{\rm c}$ determined by the gravielectric acceleration. For $r = r_{\rm c} + \delta r$ and $\phi = \phi_{\rm c} + \delta\phi$, in the zeroth-order, we have the Kepler problem equations with $E_r(r_{\rm c})$ calculated numerically in Sect. 4. The corresponding solutions are elliptic orbits. For simplicity, we will consider only the case of circular orbits $r_{\rm c}(\phi) = r_{\rm c} = const$. By substituting $E_r(r_{\rm c} + \delta r) \approx E(r_{\rm c}) + \frac{dE}{dr}(r_{\rm c})\delta r$ in Eqs. (28) and (29), we obtain

$$\frac{d^2\delta r}{dt^2} = w_0^2\delta r + 2r_{\rm c}w_0\frac{d\delta\phi}{dt} - \left.\frac{dE_r}{dr}\right|_{r_{\rm c}}\delta r - \frac{2B_z}{c}r_{\rm c}w_0,$$

$$r_{\rm c}\frac{d^2\delta\phi}{dt^2} = -2w_0\frac{d\delta r}{dt},$$

where $w_0 = \frac{d\phi_{\rm c}}{dt}$ is angular frequency, induced by gravielectric field. Thus, it can be explicitly written as $w_0^2 = \frac{E_r(r_{\rm c})}{r_{\rm c}}$. Integrating the second equation, we get

$$\frac{d\delta\phi}{dt} = -\frac{2w_0}{r_{\rm c}}\delta r,$$

where we set the integration constant to zero. Substituting this relation in the first equation, we find

$$\frac{d^2\delta r}{dt^2} = -\left(3w_0^2 + \left.\frac{dE_r}{dr}\right|_{r_{\rm c}}\right)\delta r - \frac{2B_z}{c}r_{\rm c}w_0.$$

From the numerical result, we see that $f(E)$ is positive and tends to zero at a large distance. Then, for $3\frac{E_r(r_c)}{r_c} + \frac{dE_r}{dr}\Big|_{r_c} = \Omega^2 > 0$, we find solutions

$$\delta r = -\frac{2B_z r_c w_0}{c\Omega^2} + J\sin(\Omega(t-t_0)),$$
$$\delta\phi = \delta\phi_c + \frac{4B_z w_0^2}{c\Omega^2}t + \frac{2w_0 J}{\Omega r_c}\cos(\Omega(t-t_0)),$$

where δr_c, J, and t_0 are defined by the corresponding initial conditions.

It is interesting to estimate Ω^2 at some distance r_c, e.g., $r_c = 8\,\mathrm{kpc} = 113 r_0$ which is the distance of the Sun from the center of the galaxy. Then we have $\Omega = \sqrt{0.0025 \times a_0/r_0} = 7.8 \times 10^{-16}\,\mathrm{s}^{-1}$ (the corresponding period is $T = 2.6 \times 10^8$ years), $B_z = 1.54 \times 10^{-8} a_0$, and $\delta r = -2B_z r_c w_0/c\Omega^2 = -0.8 \times 10^{-8} r_0 = -0.12\,a.u.$ The latter distance is approximately equal to 30 solar radii. The angular frequency is shifted by the value $4B_z w_0^2/c\Omega^2 = 1.1 \times 10^{-25}\,\mathrm{s}^{-1}$ (the corresponding period is $T = 1.8 \times 10^{18}$ years).

6 Conclusions

We investigated the model of DM halo with BEC core composed of ultra-light bosonic particles. Solving the generalized GPP equations for self-gravitating BEC we obtained the density profile of the DM halo and analyzed its core and envelope structure. The density and velocity profiles were found for two types of stable structures with topological charges ($s = 0$ and $s = 1$) of the BEC core.

Using this DM halo description, we investigated its gravitational field and the impact of this field on the baryonic matter. The key result of our paper is that the observable effects, predicted by the ULDM halo model, depend on the state of the core. In particular, solitonic and vortex cores yield different density and velocity distributions and thus different gravitational fields. The doughnut-like density distribution (vanishing at the vortex core) and vortex flows (rapidly increasing at the vortex axis) of the BEC core can significantly modify both gravielectric and gravimagnetic components of the gravitational field. We described the gravitational fields of these two core configurations by using the gravimagnetism approach. A dominant component of the gravitational field is the gravielectric (Newtonian) one, which generates the rotation of celestial bodies in the galaxy. The rotational velocity induced by the halo with vortex is smaller close to the core region but has the same asymptotics at large distances in comparison with the non-rotating halo.

The first post-Newtonian component of the gravitational field, which is called gravimagnetic, is induced by the rotation of the BEC vortex core and appears only in the model of a rotating halo. Although, as expected, the gravimagnetic acceleration is much weaker than the gravielectric one, it can affect the dynamics of baryonic matter in the halo, especially in its inner region. In our simplified perturbation approach for circular orbit gravimagnetic field yields radius and frequency shift, and can also induce trajectory oscillations, depending on initial conditions.

There are several possible directions in which the present study could be extended. An analysis of gravitational fields beyond the gravimagnetic approach is required in the central region of the galaxy, due to the high rotational velocity of BEC there. Furthermore, according to astrophysical observations, there is a supermassive black hole in the center of our galaxy whose presence should be taken into account. Finally, the gravitational effects of baryonic matter should be included in further studies.

Acknowledgements The authors are grateful to Yelyzaveta Nikolaieva, Sebastian Ulbricht, Stanislav Vilchinskii, and Luca Salasnich for useful discussions and comments. A.Y. acknowledge support from BIRD Project "Ultracold atoms in curved geometries" of the University of Padova. Research of E. V. Gorbar, Junji Jia and A. I. Yakimenko in this work is supported by the China-Ukraine IGSCP-12.

Data Availability Statement This manuscript has no associated data or the data will not be deposited. [Authors' comment: This is mainly a theoretical work, with a few quantities regarding the Milky Way galaxy referred from other references, but no observational data was generated.]

Funded by SCOAP^3. SCOAP^3 supports the goals of the International Year of Basic Sciences for Sustainable Development.

Appendix A

Let us discuss the self-consistency of our model, which makes use of the GEM approach to describe the first post-Newtonian contribution to the gravitational field potential. We assumed that a test particle (celestial body acted upon by the gravitational field) propagates with a non-relativistic speed v so that all terms of higher than linear order in $O(v/c)$ can be neglected in the equations of motion. As to DM, we describe it by using the nonlinear Schrödinger equation with gravitational potential Φ_g.

Since the hydrodynamical velocity in the vortex (the state with $s = 1$) is $u(r) = \alpha c r_0/r$, it increases at small r and

attains at $r \sim \alpha r_0$ values of the order of c. Obviously, the Newtonian treatment is not applicable in this region. Therefore, we use the Klein-Gordon equation in order to describe the relativistic equation of motion of bosons, as follows:

$$\nabla_\alpha \nabla^\alpha \phi + \left[\left(\frac{mc}{\hbar} \right)^2 - U(|\phi|^2) \right] \phi = 0, \tag{30}$$

where $U = \frac{2m}{\hbar^2} g N |\phi|^2$ and ϕ is the scalar field. We neglect the effective temperature because only the core region is investigated (the hydrodynamical velocity $u(r)$ is nonzero only in the core region) and ∇_α denotes covariant derivative in curved space-time.

The metric in the GEM approach reads (here all notations are the same as in Sect. 2.2)

$$\begin{aligned} dS^2 &= g_{\mu\nu} dx^\mu dx^\nu = \left(1 - \frac{2\Phi_g}{c^2}\right) (dx^0)^2 \\ &+ \frac{4}{c^2} \left(\mathbf{A}_g \mathbf{dx}\right) dx^0 + \left(-1 - \frac{2\Phi_g}{c^2}\right) \delta_{ij} dx^i dx^j \end{aligned}$$

and the Laplace operator is given by

$$\nabla_\alpha \nabla^\alpha \phi = \frac{1}{\sqrt{-g}} \partial_\alpha (\sqrt{-g} g^{\alpha\beta} \partial_\beta \phi),$$

where $g = det(g_{\mu\nu}) \approx -1$. Then we have

$$\begin{aligned} \nabla_\alpha \nabla^\alpha \phi &= \frac{1}{c^2} \left(1 - \frac{2\Phi_g}{c^2}\right) \partial_t^2 \phi - \frac{2A_g^i}{c^3} \partial_t \partial_i \phi \\ &- \frac{2}{c^3} \partial_i (A_g^i \partial_t \phi) - \partial_i \left[\left(1 + \frac{2\Phi_g}{c^2}\right) \delta^{ij} \partial_j \phi \right], \end{aligned}$$

where fields Φ_g and $\mathbf{A}_g$ are time-independent. Taking into account the gauge condition $\partial_i A_g^i = 0$, we find

$$\begin{aligned} \nabla_\alpha \nabla^\alpha \phi &= \frac{1}{c^2} \left(1 - \frac{2\Phi_g}{c^2}\right) \partial_t^2 \phi \\ &- \frac{4A_g^i}{c^3} \partial_t \partial^i \phi + \partial_i \left[\left(1 + \frac{2\Phi_g}{c^2}\right) \partial_i \phi \right]. \end{aligned}$$

To obtain a nonrelativistic approximation of the Klein-Gordon equation we represent the scalar field in the form $\phi = e^{imc^2 t/\hbar} \psi$. Substituting this expression in the Klein-Gordon equation and multiplying by $e^{-imc^2 t/\hbar}$ we get

$$\begin{aligned} &\frac{1}{c^2} \left(1 - \frac{2\Phi_g}{c^2}\right) \left[\partial_t^2 \psi + \frac{2imc^2}{\hbar} \partial_t \psi - \left(\frac{mc^2}{\hbar}\right)^2 \psi \right] \\ &- \frac{4A_g^i}{c^3} \left[\partial_t \partial^i \psi + \frac{imc^2}{\hbar} \partial^j \psi \right] + \left[1 + \frac{2\Phi_g}{c^2} \right] \partial^j \partial_j \psi \\ &+ \frac{2}{c^2} \partial^j \Phi_g \partial_j \psi + \left[\left(\frac{mc}{\hbar}\right)^2 - \frac{2m}{\hbar^2} U(|\psi|^2) \right] \psi = 0. \end{aligned}$$

Neglecting terms of order of $(u/c)^2$ and higher ($A_g \sim u/c$), we obtain

$$\begin{aligned} &\frac{2im}{\hbar} \partial_t \psi - \left(\frac{mc}{\hbar}\right)^2 \psi + 2\Phi_g \left(\frac{m}{\hbar}\right)^2 \psi + \partial^j \partial_j \psi \\ &+ \left[\left(\frac{mc}{\hbar}\right)^2 - \frac{2m}{\hbar^2} U(|\psi|^2) \right] \psi = 0 \end{aligned}$$

Finally, after some straightforward simplifications, we derive the Schrödinger equation in the form

$$i\hbar \partial_t \psi = \left(-\frac{\hbar^2}{2m} \partial^j \partial_j + m\Phi_g + U(|\psi|^2) \right) \psi.$$

Thus, we conclude that the model is self-consistent if we take into account only terms up to u/c, or, equivalently, in the region, where the hydrodynamical velocity of vortex is not relativistic ($u \ll c$).

References

1. E.G.M. Ferreira, Astron. Astrophys. Rev. **29**(1), (2021). https://doi.org/10.1007/s00159-021-00135-6
2. C.G. Böhmer, T. Harko, J. Cosmol. Astropart. Phys. **2007**(06), 025 (2007). https://doi.org/10.1088/1475-7516/2007/06/025
3. P.H. Chavanis, Eur. Phys. J. Plus **132** (2016). https://doi.org/10.1140/epjp/i2017-11544-3
4. P.H. Chavanis, T. Harko, Phys. Rev. D **86**, 064011 (2012). https://doi.org/10.1103/PhysRevD.86.064011
5. L. Hui, J.P. Ostriker, S. Tremaine, E. Witten, Phys. Rev. D **95**(4) (2017). https://doi.org/10.1103/physrevd.95.043541
6. T. Rindler-Daller, P.R. Shapiro, Mod. Phys. Lett. A **29**(02), 1430002 (2014)
7. P. Sikivie, Q. Yang, Phys. Rev. Lett. **103**(11), 111301 (2009)
8. H.Y. Schive, T. Chiueh, T. Broadhurst, Nat. Phys. **10**(7), 496 (2014). https://doi.org/10.1038/nphys2996
9. T. Matos, L.A. Ureñ a-López, Classical and Quantum Gravity **17**(13), L75 (2000). https://doi.org/10.1088/0264-9381/17/13/101
10. V. Sahni, L. Wang, Phys. Rev. D **62**, 103517 (2000). https://doi.org/10.1103/PhysRevD.62.103517
11. N. Bar, D. Blas, K. Blum, S. Sibiryakov, Phys. Rev. D **98**(8), 083027 (2018)
12. I. De Martino, T. Broadhurst, S.H.H. Tye, T. Chiueh, H.Y. Schive, Phys. Dark Univ. **28**, 100503 (2020)
13. I.S. Goldstein, S.M. Koushiappas, M.G. Walker, Phys. Rev. D **106**(6), 063010 (2022)
14. D. Harvey, R. Massey, T. Kitching, A. Taylor, E. Tittley, Science **347**(6229), 1462 (2015). https://doi.org/10.1126/science.1261381
15. J.W. Lee, S. Lim, D. Choi, arXiv e-prints arXiv:0805.3827 (2008)
16. E.J.M. Madarassy, V.T. Toth, Phys. Rev. D **91**(4), 044041 (2015). https://doi.org/10.1103/PhysRevD.91.044041
17. T. Harko, E.J. Madarassy, J. Cosmol. Astropart. Phys. **2012**(01), 020 (2012). https://doi.org/10.1088/1475-7516/2012/01/020
18. T. Harko, Phys. Rev. D **83**(12), 123515 (2011)
19. P.H. Chavanis, Phys. Rev. D **100**(8) (2019). https://doi.org/10.1103/physrevd.100.083022
20. P.H. Chavanis, Eur. Phys. J. B **95**(3), 48 (2022)
21. R. Launhardt, R. Zylka, P. Mezger, Astron. Astrophys. **384**(1), 112 (2002)

22. R. Schönrich, M. Aumer, S.E. Sale, Astrophys. J. Lett. **812**(2), L21 (2015)
23. M. Portail, O. Gerhard, C. Wegg, M. Ness, Monthly notices of the royal astronomical society p. stw2819 (2016)
24. H.Y. Schive, M.H. Liao, T.P. Woo, S.K. Wong, T. Chiueh, T. Broadhurst, W.Y.P. Hwang, Phys. Rev. Lett. **113**(26) (2014). https://doi.org/10.1103/physrevlett.113.261302
25. P.H. Chavanis, Quantum Aspects of Black Holes pp. 151–194 (2015). https://doi.org/10.1007/978-3-319-10852-0_6
26. L. Hui, A. Joyce, M.J. Landry, X. Li, J. Cosmol. Astropart. Phys. **2021**(01), 011 (2021). https://doi.org/10.1088/1475-7516/2021/01/011
27. Y.O. Nikolaieva, A.O. Olashyn, Y.I. Kuriatnikov, S.I. Vilchynskii, A.I. Yakimenko, Low Temp. Phys. **47**(8), 684 (2021). https://doi.org/10.1063/10.0005557
28. A. Dmitriev, D. Levkov, A. Panin, E. Pushnaya, I. Tkachev, Phys. Rev. D **104**(2) (2021). https://doi.org/10.1103/physrevd.104.023504
29. X. Zhang, M.H. Chan, T. Harko, S.D. Liang, C.S. Leung, Eur. Phys. J. C **78**, 1 (2018)
30. T. Rindler-Daller, P.R. Shapiro, Mon. Not. R. Astron. Soc. **422**(1), 135 (2012)
31. E.J. Madarassy, V.T. Toth, Comput. Phys. Commun. **184**(4), 1339 (2013)
32. A. Klypin, H. Zhao, R.S. Somerville, Astrophys. J. **573**(2), 597 (2002)
33. M. Walker, Planets, Stars and Stellar Systems. Volume 5: Galactic Structure and Stellar Populations **5**, 1039 (2013)
34. V.T. Toth, Int. J. Mod. Phys. D **30**(13) (2021). https://doi.org/10.1142/s0218271821501029
35. B. Mashhoon, F.W. Hehl, D.S. Theiss, Gen. Relativ. Gravit. **16**(8), 727 (1984)
36. J. Medina, R. Gilmore, *Gravitoelectromagnetism (GEM): A Group Theoretical Approach* (Drexel University, 2006). https://books.google.de/books?id=R7BSNwAACAAJ
37. B. Mashhoon. Gravitoelectromagnetism: A brief review (2003). https://doi.org/10.48550/ARXIV.GR-QC/0311030
38. R.M. Wald, *General Relativity* (Chicago Univ. Pr., Chicago, USA, 1984). https://doi.org/10.7208/chicago/9780226870373.001.0001
39. S. Sarkar, C. Vaz, L. Wijewardhana, Phys. Rev. D **97**(10), 103022 (2018)
40. K. Hayashi, I. Obata, Mon. Not. R. Astron. Soc. **491**(1), 615 (2020)
41. S. Alexander, J.J. Bramburger, E. McDonough, Phys. Lett. B **797**, 134871 (2019)
42. N. Bar, K. Blum, J. Eby, R. Sato, Phys. Rev. D **99**(10), 103020 (2019)
43. P.H. Chavanis, Phys. Dark Univ. **22**, 80 (2018). https://doi.org/10.1016/j.dark.2018.09.004. www.sciencedirect.com/science/article/pii/S2212686418301407
44. F. Guzmán, A.A. Avilez, Phys. Rev. D **97**(11) (2018). https://doi.org/10.1103/physrevd.97.116003
45. F.S. Guzman, L.A. Urena-Lopez, Astrophys. J. **645**(2), 814 (2006)
46. E. Seidel, W.M. Suen, Phys. Rev. Lett. **72**(16), 2516 (1994)
47. F. Guzmán, J. González, J. Cruz-Pérez, Phys. Rev. D **93**(10), 103535 (2016)
48. L. Posti, A. Helmi, Astron. Astrophys. **621**, A56 (2019). https://doi.org/10.1051/0004-6361/201833355
49. Y. Sofue, Publ. Astron. Soc. Jpn. **64**(4), 75 (2012). https://doi.org/10.1093/pasj/64.4.75
50. A. Obreja, T. Buck, A.V. Macciò , Astron. Astrophys. **657**, A15 (2021). https://doi.org/10.1051/0004-6361/202140983